DNA-Directed Assembly of Asymmetric Nanoclusters Using Janus Nanoparticles

Hang Xing,[†,⊥] Zidong Wang,[‡,⊥] Zhida Xu,[§] Ngo Yin Wong,[†,⊥] Yu Xiang,[†,⊥] Gang Logan Liu,[§] and Yi Lu*[,†,‡,⊥]

[†]Department of Chemistry, [‡]Department of Materials Science and Engineering, [§]Department of Electrical and Computer Engineering, and [⊥]Beckman Institute for Advanced Science and Technology, University of Illinois at Urbana—Champaign, Urbana, Illinois 61801, United States

ABSTRACT

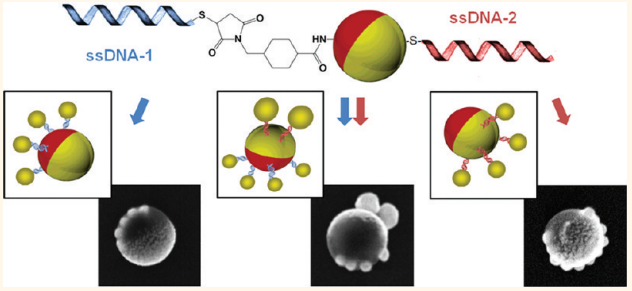

Asymmetric assembly of nanomaterials has attracted broad interests because of their unique anisotropic properties that are different from those based on the more widely reported symmetric assemblies. Despite the potential advantages, programmable fabrication of asymmetric structure in nanoscale remains a challenge. We report here a DNA-directed approach for the assembly of asymmetric nanoclusters using Janus nanoparticles as building blocks. DNA-functionalized spherical gold nanoparticles (AuNSs) can be selectively attached onto two different hemispheres of DNA-functionalized Janus nanoparticle (JNP) through DNA hybridization. Complementary and invasive DNA strands have been used to control the degree and reversibility of the assembly process through programmable base-pairing interactions, resulting in a series of modular and asymmetric nanostructures that allow systematic study of the size-dependent assembly process. We have also shown that the attachment of the AuNSs onto the gold surface of the Janus nanoparticle results in red shifting of the UV—vis and plasmon resonance spectra.

KEYWORDS: DNA · asymmetric nanocluster · self-assembly · Janus nanoparticle

With the development in nanotechnology, controlled assembly of nanoparticles into complex nanostructures has attracted extensive research attention.[1] The organization of nanoparticles into nanoscale clusters or higher dimensional structures is of great importance to realize their novel optical, electrical, and chemical properties.[2−6] In contrast to a vast majority of research efforts in symmetrical assembly, asymmetric assembly of nanomaterials is much less explored, even though the unique anisotropic properties they exhibit are not found in their symmetric counterparts.[7−10] Despite these exciting properties and promising applications of asymmetric nanostructures, controlled fabrication of these materials remains a challenge.[11] Up to now, methods of assembly to asymmetric nanostructures have been limited to either the use of an interface of different phases as steric hindrance or the formation of geometric defects in the nanoscale building blocks.[12,13] The difficulties achieving both spatial and chemical controls in previous processes limit the type, yield, and thus application of the asymmetrically assembled nanomaterials.[14,15] Therefore, there is a compelling need to develop novel methods that can make asymmetric nanostructures with uniform scale, controllable composition, and tunable properties for future applications.

A simple route to generate monodisperse, asymmetrically functionalized nanostructures is to utilize a nanoscale platform with predetermined, programmable, spatially separated functionalizations. Janus particle, which is termed from the double-faced Roman god, consists of one type of colloidal structure with two different physiochemical properties on opposite regions. This anisotropic property makes the Janus particle suitable for applications such as optical probes, two-phase stabilizers, solid surfactants, as well as building blocks for supramolecular assemblies.[16,17] Taking advantage of the asymmetric properties of Janus particles, researchers have demonstrated the assembly of dipolar and amphiphilic Janus particles through electrostatic and hydrophobic/hydrophilic interactions.[17,18] However, both of these two types of interactions are nondirectional and highly dependent on the environment. In contrast, due to high programmability through the specific Watson—Crick base pairing and ease of

* Address correspondence to yi-lu@illinois.edu.

Received for review November 5, 2011 and accepted December 8, 2011.

Published online December 08, 2011
10.1021/nn2042797

chemical and enzymatic modification,[19−21] DNA has been used as a template to position nanoscale components on double-stranded backbones in well-defined 1-D,[22,23] 2-D,[24,25] and 3-D patterns[26−28] or as a linker to attach nanoparticles, proteins, and quantum dots to direct the formation of large periodic structures.[29,30] However, DNA is much less explored for the design and assembly of asymmetric nanostructures. Most efforts so far have focused on utilizing monofunctionalized nanoparticles.[31−35] While these pioneering works demonstrated the power of directional interactions provided by DNA in templating different building blocks, the requirement of using complicated HPLC or agarose gel for purification, or using the surface of microsized magnetic particles as geometric restriction, has made it difficult to relocate different DNA strands on different regions efficiently and thus generate limited types of structures and lack of the ability to provide high yield and uniform asymmetric structures.

Herein, we report a new approach of using DNA for directing the assembly of asymmetric nanoclusters on a prefabricated JNP platform. The formation of asymmetric nanostructures with tunable optical properties has been demonstrated. We also show that DNA used as a linker between different building blocks allows programmable assembly and disassembly of Janus nanoclusters with tunable optical properties. Furthermore, the approach of incorporating DNA with Janus nanoparticles is modular and programmable. A series of asymmetric nanoclusters have been rationally designed and assembled through programmable base-pairing interactions to study the size-dependent nanoparticle self-assembly process.

RESULTS AND DISCUSSION

The fabrication of JNPs with gold covered on one hemisphere used a previously reported procedure (Figure S1 in Supporting Information).[36,37] By manipulating the duration of O_2 plasma etching, we can control the shrinkage and interparticle distance of the PS nanospheres (Figure S2a). The final diameter of PS nanospheres is around 160 nm. In order to grow a gold layer on the top surface of the PS nanoparticles, a 2 nm chromium layer and a 6 nm gold layer are deposited subsequently using an electron-beam evaporator (Figure S2b). The resulting JNPs can be released into the water solution from the surface by ultrasonication. As shown in by scanning electron microscopy (SEM, Figure S2c), monodisperse JNPs with half gold and half polystyrene were observed in high yield.

Figure 1 illustrates schematically the approach of DNA-directed assembly. A JNP with 160 nm diameter serves as the anisotropic platform for selective decoration. The active gold surface of JNPs can be functionalized with a thiolated DNA linker, ssDNA-1, while the

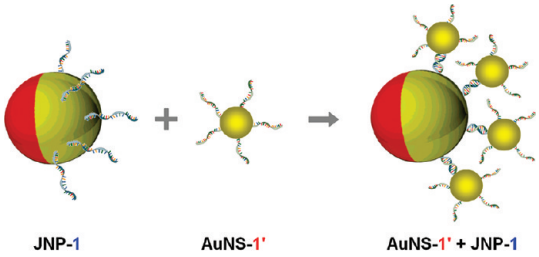

Figure 1. Schematic view of DNA-directed asymmetric self-assembly process. The gold surface of JNP is modified with thiolated ssDNA-1, while AuNS is functionalized with complementary ssDNA-1′. Asymmetric assembly occurs when thiolated ssDNA-1 pairs with complementary ssDNA-1′. For clarity, DNA molecules on nanoparticles are not shown in scale. The recognition sequences are listed below in colors.

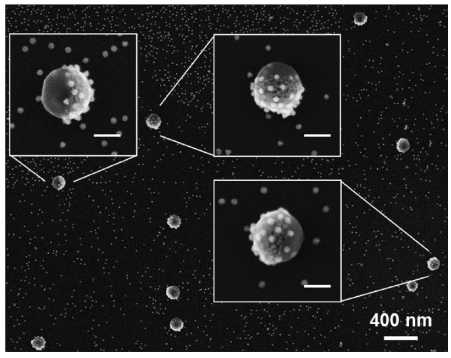

Figure 2. SEM image of asymmetric nanoclusters formed by 160 nm JNPs and 15 nm AuNSs (scale bar = 400 nm). Three nanoclusters are highlighted to illustrate the structure details. Fifteen nanometer AuNPs only attach to the gold surface of JNPs.

other polystyrene surface remains unmodified. The spatially separated regions with different chemical properties on a single JNP building block enable us to assemble asymmetric structures. To demonstrate the nanoassembly process, 15 nm AuNSs were first treated with thiolated complementary ssDNA-1′ and purified by using previously reported methods.[38,39] Two types of particles, JNP-1 and AuNS-1′, were then incubated in a ratio of 1:1000 in a buffer solution containing 5 mM HEPES buffer (pH 8.2) and 200 mM NaCl at room temperature for 24 h. During the incubation process, ssDNA-1 on JNP can hybridize to ssDNA-1′ on AuNS through a 12 base-pairing 1-1′ recognition to generate dark purple precipitates at the bottom of the test tube. SEM was employed to investigate the resulting precipitates. We observed that, on every single JNP, the gold hemisphere was occupied by a number of 15 nm AuNSs while the PS hemisphere remained largely clear of any AuNSs, resulting in asymmetric nanoclusters. Excess 15 nm AuNSs were observed in the background (Figure 2). Asymmetric nanoclusters

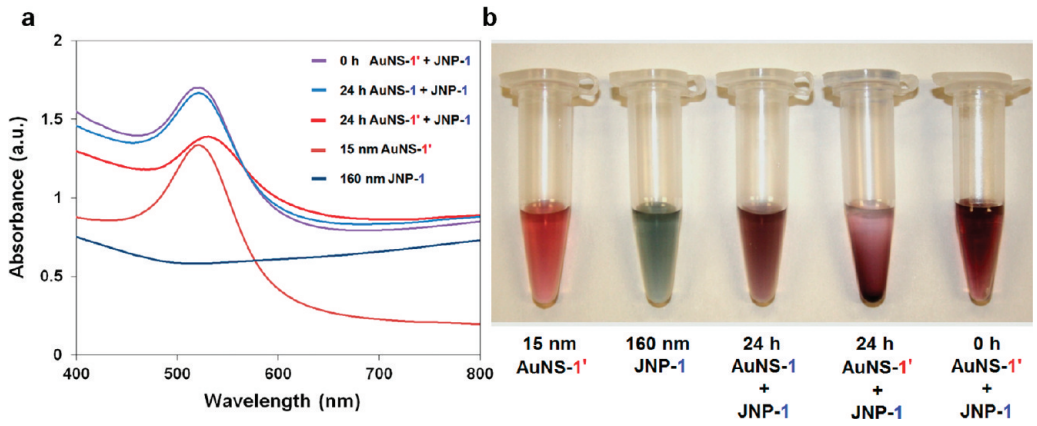

Figure 3. (a) UV−vis spectra of different solutions: 15 nm AuNS (dark red line), 160 nm JNP (dark blue line), freshly prepared mixture of JNP-1 and AuNS-1′ particles (purple line), AuNP−JNP asymmetric nanoclusters formed in assembly group after 24 h incubation and further purification (red line), and the control group, the mixture of JNP-1 and AuNS-1 particles modified with noncomplementary DNA strands after 24 h incubation (blue line). (b) Photograph images of corresponding solutions in centrifuge tubes.

could be further purified by centrifugation, removing the supernatant and rinsing the precipitates multiple times with buffer solution to remove excess 15 nm AuNSs. The TEM image (Figure S3) confirmed that most of the free AuNSs were removed and the purified asymmetric nanoclusters were uniform with 15 nm AuNSs selectively attached on the gold side but not on the PS side.

In order to understand the importance of biofunctionalization and DNA-directed nanoassembly process, we monitored the self-assembly process by ultraviolet−visible spectrophotometry (UV−vis) and photograph images of different DNA-functionalized JNP/AuNS mixtures. JNPs functionalized with ssDNA-1 (JNP-1) were incubated with 15 nm AuNSs, functionalized either with its complementary ssDNA-1′ (AuNS-1′) as the assembly group or with noncomplementary ssDNA-1 (AuNS-1) employed as a negative control group. After mixing JNP-1 particles with AuNS-1′ and AuNS-1, each in a buffer containing 5 mM HEPES buffer (pH 8.2) and 200 mM NaCl, both assembly group and negative control group displayed similar purple color initially with UV−vis absorbance centered at 520 nm (see Figure 3). Since no UV−vis absorbance is observable for JNPs in the wavelength range from 400 to 800 nm, while a standard peak at 520 nm is commonly visible for 15 nm AuNSs, we conclude that the 520 nm peak in the fresh JNP/AuNS mixtures is from the surface plasmon absorbance of free 15 nm AuNSs. After JNP/AuNS mixtures were incubated at room temperature for 24 h, the color and UV−vis spectrum of the negative control group remained almost the same as the freshly prepared sample. In contrast, the assembly group formed dark blue precipitates during the same period, with the visible peak further shifted to 535 nm and the absorption intensity lowered (Figure 3). The red shift of the spectrum is attributable to the surface plasmon coupling between localized 15 nm AuNPs and the gold surface of JNP. In order to elucidate the DNA-induced optical property change after assembly, we further employed the dark-field microscope (DFM) coupled to a CCD digital camera to investigate the light scattering property. The measurement of the localized surface plasmon resonance (LSPR) spectrum of JNP and nanoclusters was carried out by using a high-speed multispectral imaging system described in a previous paper (Figure S4).[40] Under white illumination, the AuNS−JNP asymmetric nanoclusters showed orange and light green colors (Figure S5a). The average scattering spectra obtained from multiple dots of JNPs and AuNS−JNP nanoclusters showed a similar pattern, while AuNS−JNP nanoclusters displayed an increase in scattering intensity and a red shift of approximate 30 nm relative to the unlinked JNPs (Figure S5b). Both the increased scattering and the band shift indicate the increased plasmon coupling and are consistent with the scattering properties observed previously in other multiparticle systems.[35,41−43] The asymmetric assembly can be further confirmed by comparing the SEM images of assembly group and control group. As shown in Figure 4, no AuNS and gold surface interaction was observed when noncomplementary DNA strands were used to functionalize AuNSs. These results not only indicated the recognition property of DNA molecules but also confirmed the ability of directional base-pairing interactions in guiding the assembly process of asymmetric nanostructures.

The power of DNA-directed nanoassembly lies in its programmability and reversibility. To demonstrate the use of DNA strands to control the degree and the reversibility of the asymmetric nanoassemblies, we first introduced a complementary DNA strand (cDNA-1″) with the same 12 base hybridization sequence as ssDNA-1′ into the mixture of JNP-1 and AuNS-1′ solutions to control the assembly process. Since cDNA-1″ strands are free DNA molecules in solution, the

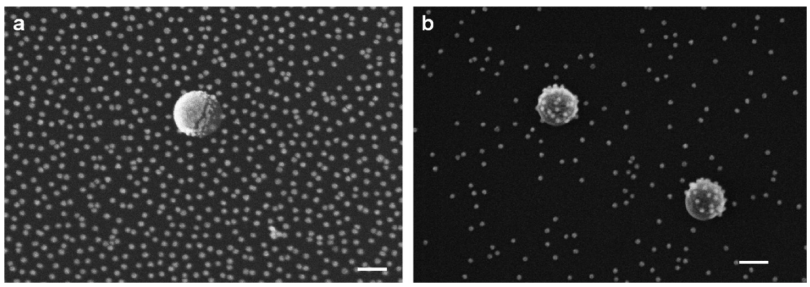

Figure 4. SEM images of the mixture of 160 nm JNPs and 15 nm AuNSs after 24 h incubation at room temperature. (a) Mixture of JNP-1 and AuNS-1. No attachment was found between AuNSs and gold surface. (b) Mixture of JNP-1 and AuNS-1′. AuNS−JNP nanoclusters were observed when using complementary DNA strands (scale bar = 100 nm).

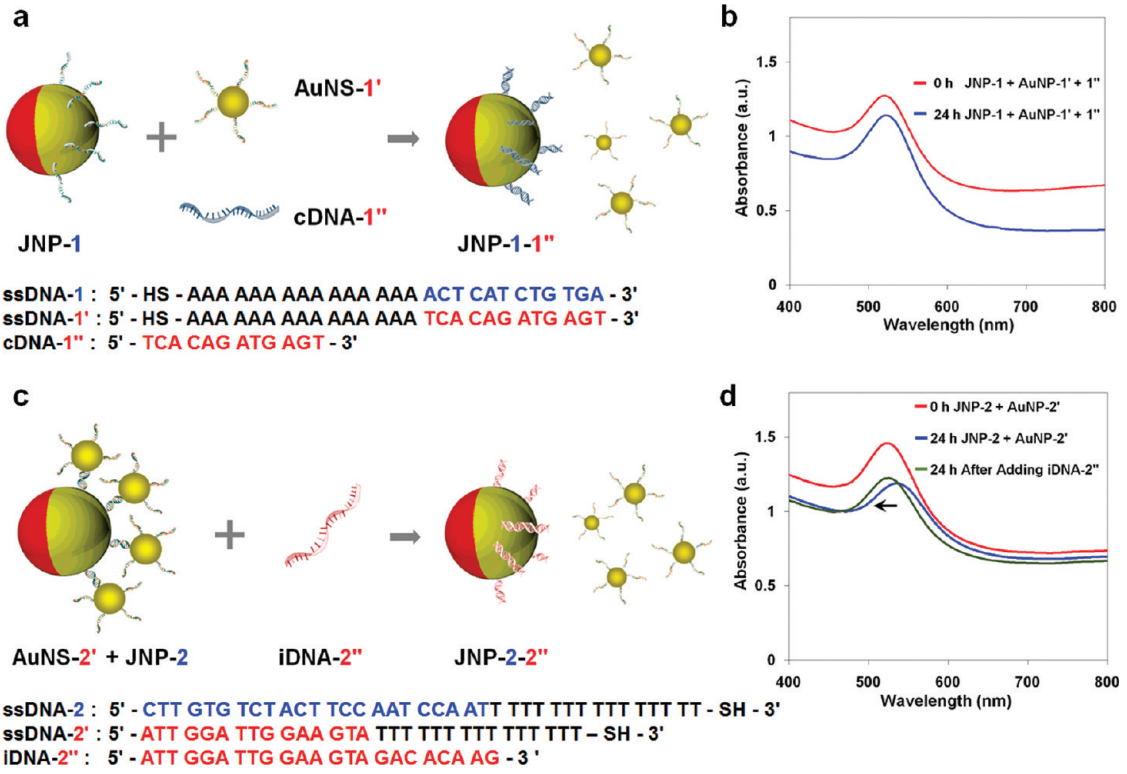

Figure 5. Schematic view of the usage of cDNA (a) and iDNA (c) for programmable control of the nanoparticle assembly and disassembly process. (b) UV−vis spectra of the mixture of JNP-1, AuNS-1′, and cDNA-1″. Freshly mixed solution (red line) showed the same peak position and similar pattern with the mixture after 24 h incubation (blue line). (d) UV−vis spectra of different solutions: freshly prepared mixture of JNP-2 and AuNS-2′ solution (red line); same solution after 24 h incubation and further purification (blue line), and the same solution after further adding iDNA-2″ with another 24 h incubation (blue line). During the whole process, the spectrum shifted to red and then shifted back.

DNA-1/cDNA-1″ hybridization should be much more facile than the DNA-1/DNA-1′ hybridization on the particle surface. Therefore, cDNA-1″ could out-compete the DNA-1′ on the AuNS for hybridization with DNA-1 on the JNP-1 and thus prevent JNP-1 and AuNS-1′ assembly (Figure 5a). As shown in Figure 5b, in the presence of cDNA-1″, the spectrum of the mixture solution remained the same and no red shift was observed. Having demonstrated the use of complementary DNA as the block agent to prevent the DNA-directed assembly process, we then wanted to show the reversible assembly and disassembly process by using an invasive DNA strand.[34] Thiolated DNA strands ssDNA-2 and ssDNA-2′ were attached onto the surface of JNPs and 15 nm AuNSs, respectively. After incubating the JNP-2 and AuNS-2′ mixture for 24 h, asymmetric nanoclusters formed through a 15 base-pairing DNA-2/DNA-2′ hybridization, similar to what was observed in Figure 3 based on DNA-1/DNA-1′ hybridization. Then, we introduced a 23-base invasive DNA strand (iDNA-2″) to release 15 nm AuNSs from the surface of JNP by replacing the DNA-2/DNA-2′ hybridization on the surface with the more stable DNA-2/iDNA-2″ hybridization (Figure 5c). As shown in Figure 5d, introducing iDNA-2″ resulted in a blue shift of the plasmon absorbance, suggesting successful disassembly of the asymmetric nanoclusters using an invasive DNA.

In order to demonstrate the generality of our approach, we applied the similar assembly process for fabrication of different asymmetric nanoclusters. AuNSs with different sizes from 15 to 80 nm were employed as nanoscale building blocks. Due to the thermodynamic instability of large AuNSs, the NaCl concentration used in the assembly was decreased to 100 mM and the incubation time was shortened from 24 to 12 h. By using AuNSs with five different sizes, a series of asymmetric nanoclusters were assembled onto the 160 nm JNP with well-controlled morphology and yield (Figure 6). Consistent with the prediction, with the increase of AuNS size, the number of AuNSs on each JNP decreased. Interestingly, although asymmetric nanoclusters can be observed in different orientations under SEM, the top view of nanoclusters with the PS hemisphere on the bottom is very rare. We hypothesized that gold hemisphere is more likely to precipitate onto the silicon substrate during the adsorption process since the attached AuNSs make it much heavier than the PS site.

A representative statistical analysis of different asymmetric nanoclusters has been achieved based on SEM and TEM images (Figure 7a). The analysis illustrates that, within a certain number range, different AuNSs can be attached onto the JNP platform with narrow number distribution (Figure S6). The results further demonstrate that our approach is modular to extend to different building blocks, producing products with high yield. To obtain deeper insight into the size-dependent self-assembly process, we used a theoretical model based on hexagonal closed-packing structure to calculate the number of AuNSs on each JNP. Effective diameters of DNA-capped particles were calculated based on a reported worm-like chain model.[44] The calculated results accurately represented the experimentally observed changing trend (Figure 7b).

We further investigated the surface assembly degree by comparing the ratio of experimental number of AuNSs to the theoretical number of AuNSs on a single JNP for different size AuNSs. Interestingly, we found that, although the surface assembly degrees for different size AuNS are all ~50% of the predicted by calculation, a trend exists. As illustrated in Figure 7c, 15 nm AuNSs possess the highest self-assembly degree, while 80 nm AuNPs have the lowest one. The differences between the experimental and theoretical results might be due to AuNPs being randomly attached to the gold surface. Unlike a hexagonal closed-packing model, the random attachment process of AuNPs results in large empty spaces between particles. Therefore, it is easier for small AuNPs to further occupy these empty spaces and thus reach a high surface assembly degree (Figure S7).

Taking advantage of the asymmetric structure, prefabricated JNPs can be further modified with spatially separated different DNA strands, providing a powerful platform for the assembly of novel nanostructures. To provide functional groups on the PS hemisphere of JNP, 200 nm amine-modified PS nanospheres were utilized to fabricate amine-modified JNPs through the same procedure mentioned above. After the gold deposition process, half of the amine-modified PS area was covered by gold, while the other half was protected and the remaining amine groups are still functional. Two types of thiolated DNA strands, ssDNA-2 and ssDNA-3, were employed to modify two separate surface of JNP (Figure 8a). DNA-2 was first modified

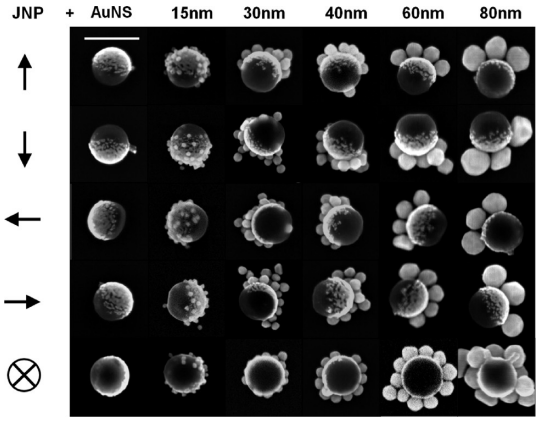

Figure 6. SEM images of representative asymmetric nanoclusters in different orientations (scale bar = 200 nm).

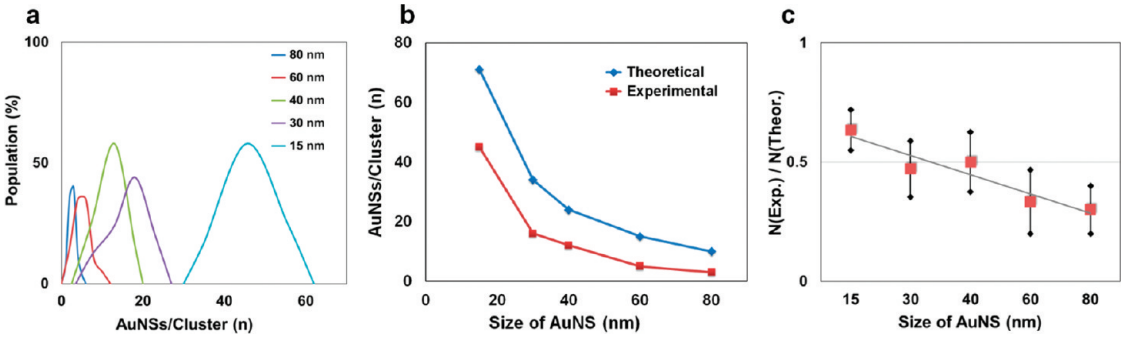

Figure 7. (a) Statistical analysis of the number of AuNSs per nanocluster. (b) Comparison of theoretical and experimental number of AuNSs per cluster. (c) Diagram of the relationship between surface assembly degree and the size of AuNS.

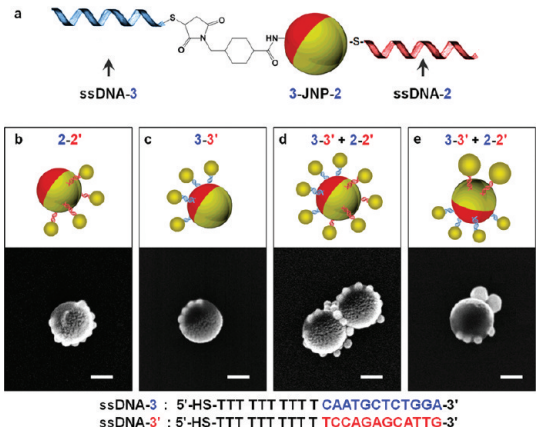

Figure 8. (a) Schematic view of two different coupling chemistries on the surface of an amine-modified 200 nm JNP. (b–e) Schematic views and SEM images of representative asymmetric nanoclusters formed by dual DNA-functionalized JNP and different DNA-encoded AuNSs: (b) 40 nm AuNS-2′, (c) 40 nm AuNS-3′, and (d) equal mixture of 40 nm AuNS-2′ and AuNS-3′; (e) equal mixture of 80 nm AuNS-2′ and 40 nm AuNS-3′ (scale bar = 100 nm).

onto the gold hemisphere through gold–thiol interaction. After purification, ssDNA-3 was then covalently attached to the amine-modified polymer hemisphere *via* sulfo-SMCC coupling, forming a dual DNA-functionalized JNP (3-JNP-2). To demonstrate the dual functionalizations and potential novel assembly, different sized AuNSs, functionalized with ssDNA-2′ or ssDNA-3′, were prepared, respectively. After incubating the JNP with 40 nm AuNS-2′, AuNSs were selectively attached onto the gold hemisphere through DNA-2/DNA-2′ hybridization (Figure 8b). However, if JNP was incubated with 40 nm AuNS-3′, few AuNSs could be found on the gold hemisphere. Instead, AuNSs were selectively immobilized onto the PS hemisphere, indicating the 3-3′ DNA recognition (Figure 8c). If JNP was incubated with an equal mixture of 40 nm AuNS-2′ and AuNS-3′, JNP was found to be surrounded by 40 nm AuNSs in all directions (Figure 8d). Furthermore, if two different sized AuNSs with appropriate DNA modifications were introduced to attach to JNP, a novel trivalent asymmetric nanocluster was formed with 80/60 nm AuNSs-2′ on the gold site and 40/30 nm AuNSs-3′ on the other side (Figure 8e and Figure S8). These results further indicate the power of DNA-directed nanoassembly. By simply encoding AuNSs with different DNA strands, we could selectively modify the target region on JNP in a well-controlled manner.

CONCLUSION

In conclusion, we have demonstrated for the first time that DNA can be used for directing the assembly of asymmetric nanoclusters on the prefabricated JNP platform. Both cDNA and iDNA can be used to tune the assembly and disassembly of particles, indicating that DNA plays an essential role for programmable control the self-assembly process. Furthermore, this approach has been applied to construct a series of asymmetric nanoclusters. A theoretical model has also been established to systematically study the size-dependent assembly process. By taking advantage of a simple fabrication technique, we can generate Janus nanoparticles (JNPs) with high yield and promote directed self-assembly with DNA modification. We have shown that our approach is modular. The combination of DNA linkers and JNPs provides both spatial and chemical control over the assembly process. This new strategy for the synthesis of using monodisperse DNA-functionalized JNPs is a promising route for construction of many different asymmetric structures with spatially separated functionalities for potential photonic, electronic, and biomedical applications.

METHODS

Chemicals and Materials. (3-Aminopropyl)triethoxysilane (APTES, $C_9H_{23}NO_3Si$, 97%), tris(2-carboxyethyl)phosphine hydrochloride (TCEP, $C_9H_{15}O_6P \cdot HCl$), and 4-(*N*-maleimidomethyl)cyclohexane-1-carboxylic acid 3-sulfo-*N*-hydroxysuccinimide ester sodium salt (sulfo-SMCC, $C_{16}H_{17}N_2NaO_9S$) were purchased from Sigma-Aldrich and used without further purification. Gold nanosphere (AuNSs) solutions with 15, 30, 40, 60, and 80 nm diameter were purchased from Ted Pella (Redding, CA) and purified by centrifugation before use. Plain and amine-modified polystyrene nanospheres with 200 nm diameter were purchased from Polysciences (Warrington, PA). All oligonucleotides used in this study were purchased from Integrated DNA Technologies Inc. (Coralville, IA), with following sequences:

ssDNA-1: 5′-HS-$(A)_{15}$-ACTCATCTGTGA-3′
ssDNA-1′: 5′-HS-$(A)_{15}$TCACAGATGAGT-3′
cDNA-1″: 5′-TCACAGATGAGT-3′
ssDNA-2: 5′-CTTGTGTCTACTTCCAATCCAAT-$(T)_{15}$-SH-3′
ssDNA-2′: 5′-ATTGGATTGGAAGTA-$(T)_{15}$-SH-3′
iDNA-2″: 5′-ATTGGATTGGAAGTAGACACAAG-3′
ssDNA-3: 5′-HS-$(T)_{10}$-CAATGCTCTGGA-3′
ssDNA-3′: 5′-HS-$(T)_{10}$-TCCAGAGCATTG-3′

Fabrication of Janus Nanoparticle. The fabrication begins with the formation of a 200 nm polystyrene (PS) nanosphere monolayer. The glass substrates (3 in. × 1 in. × 1 mm, Fisher Scientific, PA) were cleaned in piranha solution for 2 h and then carefully rinsed with deionized water and anhydrous ethanol subsequently. The clean glass slides were incubated into 1% 3-aminopropyltriethoxysilane (APTES) ethanol solution for 12 h to form a homogeneous APTES film. The APTES-covered glass substrates were then rinsed with ethanol and dried by nitrogen gas. The 200 nm PS nanosphere solution was first 1:30 diluted in 5 mM HEPES buffer (HEPES = 4-(2-hydroxyethyl)-1-piperazineethane sulfonic acid, pH = 7.0, 1 mM citrate), then dropped onto the APTES-covered glass substrate. After 1 h incubation, the glass substrates were rinsed with deionized water to form a monolayer of PS nanospheres by removing excess PS nanospheres. Completely dried substrates were then loaded into a nondirectional oxygen plasma etching system (March Plasmod, 250 W) to tune the PS nanosphere size by varying the etching time. Metal evaporation (Cr/Au, 2 nm/6 nm) was then performed on the monolayer of PS nanospheres (Temescal six pocket e-beam evaporation system) to obtain the monolayer of JNPs. All JNPs were further released from the surface by immersing the glass substrates in deionized water and

sonicating for 2 min. The concentration of obtained JNP solution is about 0.2 nM.

Preparation of Thiolated DNA-Functionalized AuNSs and JNPs. Functionalization of thiolated DNA on 15 nm gold nanospheres was carried out by following a previous published protocol with some modifications.[38,39] Briefly, 3 μL of 1 mM thiolated DNA was first mixed with 0.5 μL of 10 mM TCEP solution and 0.4 μL of 500 mM acetate buffer (pH 5.2) to activate the thiolated DNA. After 1 h incubation, the mixture was then transferred into 1 mL of 15 nm AuNS solution (10 nM) followed by incubation overnight. The mixture solution was then added to 500 mM Tris acetate buffer (pH 8.2) to bring the buffer concentration to 5 mM. The solution was left to anneal for another 24 h after gradually increasing the NaCl concentration to 100 mM over 1 h. To purify the nanospheres from the unreacted DNA, the excess DNA strands were removed from the solution by centrifugation at 16 110*g* for 15 min.

Functionalization of thiolated DNA on larger AuNSs (30, 40, 60, and 80 nm) and JNPs was carried out in an analogous process. Sonication and magnetic stirring was applied to prevent precipitation and facilitate the reaction.

Preparation of Dual DNA-Functionalized JNPs. Amine-modified JNPs were first functionalized with thiolated DNA-2 onto a gold hemisphere by using the above-mentioned process. For functionalization of DNA-3 onto the amine-modified PS hemisphere, JNP was dispersed in buffer A into 0.2 nM. Sulfo-SMCC of 1 mg was added into 500 μL JNP solution and then placed on a shaker for 1 h at room temperature. The insoluble excess sulfo-SMCC was removed from solution, and the sulfo-SMCC-activated JNP was purified by using buffer A five times. The purified sulfo-SMCC-activated JNP was mixed, and the activated thiol-DNA-3 solution gently shaken for 1 min. The mixture was then incubated at room temperature for 48 h. The final solution was applied to Amicon-100K eight times using buffer A without Tween-20 to remove any unreacted DNA-3.

Buffer A: 0.1 M NaCl, 0.1 M sodium phosphate buffer, pH 7.3.

Assembly of Thiolated DNA-Functionalized JNPs and AuNSs. The assembly of 15 nm AuNS–JNP clusters was performed in a 1.5 mL centrifuge tube in 5 mM Tris acetate buffer (pH 8.2) and 200 mM NaCl. AuNSs (10 nM) and JNPs functionalized with complementary thiolated DNA strands were mixed in a concentration ratio of 500:1 and incubated for 24 h at room temperature to allow assembly. During this process, the color of the mixture solution gradually decreased from dark purple to optically transparent with blue precipitates formed at the bottom of the centrifuge tube. After incubation, the AuNS–JNP mixture solution was centrifuged at 2000*g* for 5 min to remove the free 15 nm AuNSs in the supernatant, and the blue precipitates were redispersed in buffer solution (5 mM Tris acetate, pH 8.2, 100 mM NaCl) for further characterization. The assembly of larger AuNS–JNP clusters was followed by a similar process with the exception of lower AuNS concentration ratios. Salt concentration and incubation time were decreased to 100 mM and 12 h, respectively.

The assembly and disassembly of AuNS–JNP clusters was achieved in identical buffer conditions to cluster fabrication mentioned above. Complementary DNA (cDNA) strands and invasive DNA strands were used to manipulate the assembly process. For the usage of cDNA, 10 μL of 100 mM cDNA was added into the buffer solution together with thiolated DNA-functionalized JNPs and AuNSs before the incubation. For the usage of iDNA, the final assembled blue precipitates were redispersed in fresh buffer and 10 μL of 1 M iDNA was added followed by incubation for 6–12 h at room temperature with gentle stirring. All of the assembly processes can be monitored by UV–vis adsorption.

Characterization Methods. The size and morphology of nanoparticles as well as the nanoassembly structures were analyzed using a JEOL 2010LaB6 transmission electron microscope (TEM) and a Hitachi S4800 high-resolution scanning electron microscopy (SEM). Samples were prepared by drop-casting nanoparticle solutions onto a carbon-coated copper TEM grid or a silicon wafer (Ted Pella), followed by removing excess solution with filter paper after 10 min.

The UV–vis spectra of the nanoparticles and asymmetric nanoclusters were collected on a Hewlett-Packard 8453 UV–vis spectrophotometry. Dark-field light scattering images of nanoclusters were acquired using a Zeiss Axiovert 200 M inverted microscope with an EC Epiplan 50× HD objective (NA = 0.7) and CCD camera. The digital camera was white-balanced by using Zeiss Axiovision software before data acquisition. Therefore, the color observed in the digital images represented the true color of the scattered light. The localized surface plasmon resonance spectra were collected on a self-built multispectral dark-field imaging system with a 0.42 NA objective.

Measurement of Localized Surface Plasmon Resonance Spectrum. For single particle plasmon resonance scattering spectroscopy, a multispectral dark-field imaging technique with high-speed and high-throughput was established based on previously reported method.[40] Compared with conventional spectrometry of single particle scattering, which relies on white light illumination and spectrograph, thus an aperture is needed and the distribution of particles has to be sparse enough to capture the scattering spectra of single particle at one time, this multispectral imaging system utilizes a sweeping monochromatic light source along with a dark-field condenser for illumination and a camera synchronized with the sweeping wavelengths for recording the intensity for all particles in the whole field of vision simultaneous. The scattering spectrum of each particle is plotted by its intensity in each frame with respect to its corresponding wavelength. In that case, spectra of all particles in the field of vision can be captured in a short time with no aperture needed, and the sparseness of particles is not rigorously required. In our measurement, the monochromator swept from 400 to 700 nm with the step of 2 nm and standing or exposure time of 3000 ms for each wavelength. The whole capturing process took 7.5 min. In order to calibrate the light source and instrumental bias, all particle scattering spectra were corrected by the scattering spectrum of polystyrene particles with the diameter of 200 nm, which is supposed to have no resonance or peaks according to Mie theory. Scattering spectra were corrected and normalized before comparison.

Acknowledgment. We thank Professor Catherine Murphy for advice and helpful discussions. This work has been supported by the National Science Foundation Center for Nanoscale Chemical-Electrical-Mechanical Manufacturing Systems (Nano-CEMMS) under NSF Award #0749028 (CMMI). Scanning electron microscopy and transmission emission microscopy were carried out at the Center for Microanalysis of Materials, University of Illinois, which is partially supported by the U.S. Department of Energy under Grant DEFG02-91-ER45439.

Supporting Information Available: Experimental details and additional figures. This material is available free of charge *via* the Internet at http://pubs.acs.org.

REFERENCES AND NOTES

1. Whitesides, G. M.; Grzybowski, B. Self-Assembly at All Scales. *Science* **2002**, *295*, 2418–2421.
2. Mirkin, C. A.; Letsinger, R. L.; Mucic, R. C.; Storhoff, J. J. A DNA-Based Method for Rationally Assembling Nanoparticles into Macroscopic Materials. *Nature* **1996**, *382*, 607–609.
3. Redl, F. X.; Cho, K. S.; Murray, C. B.; O'Brien, S. Three-Dimensional Binary Superlattices of Magnetic Nanocrystals and Semiconductor Quantum Dots. *Nature* **2003**, *423*, 968–971.
4. Fu, A.; Micheel, C. M.; Cha, J.; Chang, H.; Yang, H.; Alivisatos, A. P. Discrete Nanostructures of Quantum Dots/Au with DNA. *J. Am. Chem. Soc.* **2004**, *126*, 10832–10833.
5. Wang, F.; Han, Y.; Lim, C. S.; Lu, Y. H.; Wang, J.; Xu, J.; Chen, H. Y.; Zhang, C.; Hong, M. H.; Liu, X. G. Simultaneous Phase and Size Control of Upconversion Nanocrystals through Lanthanide Doping. *Nature* **2010**, *463*, 1061–1065.
6. Chen, G.; Wang, Y.; Yang, M. X.; Xu, J.; Goh, S. J.; Pan, M.; Chen, H. Y. Measuring Ensemble-Averaged Surface-Enhanced Raman Scattering in the Hotspots of Colloidal Nanoparticle Dimers and Trimers. *J. Am. Chem. Soc.* **2010**, *132*, 3644–3645.

7. Verma, A.; Uzun, O.; Hu, Y. H.; Hu, Y.; Han, H. S.; Watson, N.; Chen, S. L.; Irvine, D. J.; Stellacci, F. Surface-Structure-Regulated Cell-Membrane Penetration by Monolayer-Protected Nanoparticles. *Nat. Mater.* **2008**, *7*, 588–595.
8. Maier, S. A.; Brongersma, M. L.; Kik, P. G.; Meltzer, S.; Requicha, A. A. G.; Atwater, H. A. Plasmonics—A Route to Nanoscale Optical Devices. *Adv. Mater.* **2001**, *13*, 1501–1505.
9. Hu, S. H.; Gao, X. H. Nanocomposites with Spatially Separated Functionalities for Combined Imaging and Magnetolytic Therapy. *J. Am. Chem. Soc.* **2010**, *132*, 7234–7237.
10. Zhang, Y.; Barhoum, A.; Lassiter, J. B.; Halas, N. J. Orientation-Preserving Transfer and Directional Light Scattering from Individual Light-Bending Nanoparticles. *Nano Lett.* **2011**, *11*, 1838–1844.
11. DeVries, G. A.; Brunnbauer, M.; Hu, Y.; Jackson, A. M.; Long, B.; Neltner, B. T.; Uzun, O.; Wunsch, B. H.; Stellacci, F. Divalent Metal Nanoparticles. *Science* **2007**, *315*, 358–361.
12. Xia, Y.; Yang, P.; Sun, Y.; Wu, Y.; Mayers, B.; Gates, B.; Yin, Y.; Kim, F.; Yan, H. One-Dimensional Nanostructures: Synthesis, Characterization, and Applications. *Adv. Mater.* **2003**, *15*, 353–389.
13. McConnell, M. D.; Kraeutler, M. J.; Yang, S.; Composto, R. J. Patchy and Multiregion Janus Particles with Tunable Optical Properties. *Nano Lett.* **2010**, *10*, 603–609.
14. Brown, L. V.; Sobhani, H.; Lassiter, J. B.; Nordlander, P.; Halas, N. J. Heterodimers: Plasmonic Properties of Mismatched Nanoparticle Pairs. *ACS Nano* **2010**, *4*, 819–832.
15. Maye, M. M.; Kumara, M. T.; Nykypanchuk, D.; Sherman, W. B.; Gang, O. Switching Binary States of Nanoparticle Superlattices and Dimer Clusters by DNA Strands. *Nat. Nanotechnol.* **2010**, *5*, 116–120.
16. Roh, K. H.; Martin, D. C.; Lahann, J. Biphasic Janus Particles with Nanoscale Anisotropy. *Nat. Mater.* **2005**, *4*, 759–763.
17. Jiang, S.; Chen, Q.; Tripathy, M.; Luijten, E.; Schweizer, K. S.; Granick, S. Janus Particle Synthesis and Assembly. *Adv. Mater.* **2010**, *22*, 1060–1071.
18. Hong, L.; Cacciuto, A.; Luijten, E.; Granick, S. Clusters of Charged Janus Spheres. *Nano Lett.* **2006**, *6*, 2510–2514.
19. Storhoff, J. J.; Mirkin, C. A. Programmed Materials Synthesis with DNA. *Chem. Rev.* **1999**, *99*, 1849–1862.
20. Seeman, N. C. DNA in a Material World. *Nature* **2003**, *421*, 427–431.
21. Katz, E.; Willner, I. Integrated Nanoparticle−Biomolecule Hybrid Systems: Synthesis, Properties, and Applications. *Angew. Chem., Int. Ed.* **2004**, *43*, 6042–6108.
22. Alivisatos, A. P.; Johnsson, K. P.; Peng, X.; Wilson, T. E.; Loweth, C. J.; Bruchez, M. P.; Schultz, P. G. Organization of 'Nanocrystal Molecules' Using DNA. *Nature* **1996**, *382*, 609–611.
23. Ding, B. Q.; Deng, Z. T.; Yan, H.; Cabrini, S.; Zuckermann, R. N.; Bokor, J. Gold Nanoparticle Self-Similar Chain Structure Organized by DNA Origami. *J. Am. Chem. Soc.* **2010**, *132*, 3248–3249.
24. Zheng, J. W.; Constantinou, P. E.; Micheel, C.; Alivisatos, A. P.; Kiehl, R. A.; Seeman, N. C. Two-Dimensional Nanoparticle Arrays Show the Organizational Power of Robust DNA Motifs. *Nano Lett.* **2006**, *6*, 1502–1504.
25. Pinto, Y. Y.; Le, J. D.; Seeman, N. C.; Musier-Forsyth, K.; Taton, T. A.; Kiehl, R. A. Sequence-Encoded Self-Assembly of Multiple-Nanocomponent Arrays by 2D DNA Scaffolding. *Nano Lett.* **2005**, *5*, 2399–2402.
26. Park, S. Y.; Lytton-Jean, A. K. R.; Lee, B.; Weigand, S.; Schatz, G. C.; Mirkin, C. A. DNA-Programmable Nanoparticle Crystallization. *Nature* **2008**, *451*, 553–556.
27. Nykypanchuk, D.; Maye, M. M.; van der Lelie, D.; Gang, O. DNA-Guided Crystallization of Colloidal Nanoparticles. *Nature* **2008**, *451*, 549–552.
28. Sharma, J.; Chhabra, R.; Cheng, A.; Brownell, J.; Liu, Y.; Yan, H. Control of Self-Assembly of DNA Tubules through Integration of Gold Nanoparticles. *Science* **2009**, *323*, 112–116.
29. Aldaye, F. A.; Palmer, A. L.; Sleiman, H. F. Assembling Materials with DNA as the Guide. *Science* **2008**, *321*, 1795–1799.
30. Tan, S. J.; Campolongo, M. J.; Luo, D.; Cheng, W. Building Plasmonic Nanostructures with DNA. *Nat. Nanotechnol.* **2011**, *6*, 268–276.
31. Claridge, S. A.; Goh, S. L.; Frechet, J. M. J.; Williams, S. C.; Micheel, C. M.; Alivisatos, A. P. Directed Assembly of Discrete Gold Nanoparticle Groupings Using Branched DNA Scaffolds. *Chem. Mater.* **2005**, *17*, 1628–1635.
32. Xu, X.; Rosi, N. L.; Wang, Y.; Huo, F.; Mirkin, C. A. Asymmetric Functionalization of Gold Nanoparticles with Oligonucleotides. *J. Am. Chem. Soc.* **2006**, *128*, 9286–9287.
33. Mastroianni, A. J.; Claridge, S. A.; Alivisatos, A. P. Pyramidal and Chiral Groupings of Gold Nanocrystals Assembled Using DNA Scaffolds. *J. Am. Chem. Soc.* **2009**, *131*, 8455–8459.
34. Maye, M. M.; Nykypanchuk, D.; Cuisinier, M.; van der Lelie, D.; Gang, O. Stepwise Surface Encoding for High-Throughput Assembly of Nanoclusters. *Nat. Mater.* **2009**, *8*, 388–391.
35. Sheikholeslami, S.; Jun, Y.-W.; Jain, P. K.; Alivisatos, A. P. Coupling of Optical Resonances in a Compositionally Asymmetric Plasmonic Nanoparticle Dimer. *Nano Lett.* **2010**, *10*, 2655–2660.
36. Perro, A.; Reculusa, S.; Ravaine, S.; Bourgeat-Lami, E.; Duguet, E. Design and Synthesis of Janus Micro- and Nanoparticles. *J. Mater. Chem.* **2005**, *15*, 3745–3760.
37. Wu, L. Y.; Ross, B. M.; Hong, S.; Lee, L. P. Bioinspired Nanocorals with Decoupled Cellular Targeting and Sensing Functionality. *Small* **2010**, *6*, 503–507.
38. Demers, L. M.; Mirkin, C. A.; Mucic, R. C.; Reynolds, R. A.; Letsinger, R. L.; Elghanian, R.; Viswanadham, G. A Fluorescence-Based Method for Determining the Surface Coverage and Hybridization Efficiency of Thiol-Capped Oligonucleotides Bound to Gold Thin Films and Nanoparticles. *Anal. Chem.* **2000**, *72*, 5535–5541.
39. Liu, J.; Lu, Y. Preparation of Aptamer-Linked Gold Nanoparticle Purple Aggregates for Colorimetric Sensing of Analytes. *Nat. Protoc.* **2006**, *1*, 246–252.
40. Liu, G. L.; Doll, J. C.; Lee, L. P. High-Speed Multispectral Imaging of Nanoplasmonic Array. *Opt. Express* **2005**, *13*, 8520–8525.
41. Reinhard, B. M.; Sheikholeslami, S.; Mastroianni, A.; Alivisatos, A. P.; Liphardt, J. Use of Plasmon Coupling To Reveal the Dynamics of DNA Bending and Cleavage by Single EcoRV Restriction Enzymes. *Proc. Natl. Acad. Sci. U.S.A.* **2007**, *104*, 2667–2672.
42. Sebba, D. S.; Mock, J. J.; Smith, D. R.; LaBean, T. H.; Lazarides, A. A. Reconfigurable Core−Satellite Nanoassemblies as Molecularly-Driven Plasmonic Switches. *Nano Lett.* **2008**, *8*, 1803–1808.
43. Chen, J. I. L.; Chen, Y.; Ginger, D. S. Plasmonic Nanoparticle Dimers for Optical Sensing of DNA in Complex Media. *J. Am. Chem. Soc.* **2010**, *132*, 9600–9601.
44. Rivetti, C.; Walker, C.; Bustamante, C. Polymer Chain Statistics and Conformational Analysis of DNA Molecules with Bends or Sections of Different Flexibility. *J. Mol. Biol.* **1998**, *280*, 41–59.